Title: Uncovering a role for the dorsal hippocampal commissure in episodic memory

Authors: Postans M*[1,2], Parker GD[1,3], Lundell H[4], Ptito M[5], Hamandi K[1,6,7,9], Gray WP[1,6,7,9], Aggleton JP[1,2], Dyrby TB[4,10], Jones DK[1,2,9,11], Winter M[1,2,9, 12]

1. Cardiff University Brain Research Imaging Centre (CUBRIC), School of Psychology, Cardiff University, Cardiff, UK
2. School of Psychology, Cardiff University, Cardiff UK
3. Experimental MRI Centre (EMRIC), School of Biosciences, Cardiff University, Cardiff, UK
4. Danish Research Centre for Magnetic Resonance, Centre for Functional and Diagnostic Imaging and Research, Copenhagen University Hospital Hvidovre, Hvidovre, Denmark
5. School of Optometry, University of Montreal, Montreal, Canada and Department of Neurology and Neurosurgery, Montreal Neurological Institute, Montreal, Canada
6. The Alan Richens Welsh Epilepsy Centre, Department of Neurology, University Hospital of Wales, Cardiff UK
7. Institute of Psychological Medicine and Clinical Neurosciences, School of Medicine, Cardiff University, Cardiff, UK
8. Dept of Neurosurgery, Neurosciences Division, University Hospital Wales, Cardiff, UK
9. Brain Repair And Intracranial Neurotherapeutics (BRAIN) Unit, School of Medicine, Cardiff University, Cardiff, UK
10. Department of Applied Mathematics and Computer Science, Technical University of Denmark, Kongens, Lyngby, Denmark
11. School of Psychology, Australian Catholic University, Melbourne, Australia
12. Department of Clinical Neuropsychology, University Hospital of Wales, Cardiff, UK

Keywords: hippocampal commissure, tractography, episodic memory, familiarity, recollection

26 *** Corresponding Author:** Dr Mark Postans

27 **Address:** Cardiff University Brain Research Imaging Centre (CUBRIC), School of Psychology, Cardiff

28 University, Maindy Road, Cardiff, CF24 4HQ

29

30 **Email:** postansm@cardiff.ac.uk

Abstract

The dorsal hippocampal commissure (DHC) provides inter-hemispheric connections between temporal lobe brain regions but there is scant evidence of a role for the DHC in successful memory performance. We used diffusion-weighted MRI (DW-MRI) and white matter tractography to reconstruct the DHC across both humans and nonhuman primates, and show close consistency between these tract reconstructions and the known anatomy. Anterograde tract tracer evidence highlighted the parahippocampal origins of DHC fibers in nonhuman primates. Finally, we derived Diffusion Tensor Magnetic Resonance Imaging (DT-MRI) measures of white matter microstructure in 100 human subjects, and found that the mean diffusivity of the DHC was correlated with performance in a standardised episodic memory task. These findings highlight, for the first time, the DHC as an anatomically distinct tract with a potential role in episodic memory. Our tract reconstruction approach may facilitate further understanding of the role of the DHC in both health and disease.

Introduction

The two hemispheres of the brain are connected by commissural fiber systems that include the corpus callosum, anterior commissure (AC), posterior commissure, ventral hippocampal commissure (VHC), and dorsal hippocampal commissure (DHC)[1]. The DHC (alternatively the 'dorsal psaltarium') provides inter-hemispheric connections between functionally-related structures in the medial temporal lobes (MTL), including the presubiculum, entorhinal and parahippocampal cortex[1–3]. Given that these regions play a key role in successful learning and memory[4–7], their ability to communicate effectively with contralateral homologous regions via the DHC may also be important for performance in these cognitive domains.

There have, however, been few studies of the function of the DHC, potentially due to misunderstanding around the cross-species anatomy of the DHC, as distinct from other local fiber populations such as the VHC, fornix, and corpus callosum[1,8,9]. In rodents, the VHC supports dense inter-hemispheric connections between the hippocampi, which originate throughout the long-axis of the hippocampus; in nonhuman primates, VHC connections are reduced so that only the uncal and genual subdivisions of the hippocampal formation are connected to those in the contralateral hemisphere[1,3]. By contrast, the DHC remains a substantial tract in nonhuman primates, but it carries commissural projections to and from the parahippocampal region rather than the hippocampus proper. From injection sites in the presubiculum, entorhinal and parahippocampal cortex, tract tracer studies in nonhuman primates have traced labelled DHC fibers into the alveus and fimbria and then the posterior columns of the fornix; these fibers arch dorso-anteriorly and then turn medially to cross the midline along the inferior aspect of the corpus callosum, before taking a mirror-image route back to the contralateral parahippocampal region[1,2]. Anatomical studies have found no convincing evidence of a VHC in humans but the location of the human DHC corresponds precisely to that reported for nonhuman primates[3]. Despite their distinct anatomy, the VHC and DHC are sometimes collectively termed 'the hippocampal commissure'[1], and the DHC is sometimes described as part of the fornix (e.g., 'fornix commissure')[10]. It is, however, difficult to infer the function of the DHC from potentially informative clinical case reports and animal studies if it is not appropriately differentiated from these other structures.

In one relevant study highlighting a potential role for the DHC in successful learning and memory, fornix transection did not impair the ability of monkeys to learn concurrent visual discriminations, but the fornix damage in one subject extended to the DHC, and that subject made significantly more errors and required more training sessions to learn the task compared to the slowest control[11]. This subject was also impaired in an object recognition task[12]. Similarly, clinical case reports describe individuals with anterograde amnesia following combined DHC and fornix damage[13,14], although it is difficult to evaluate the effect of DHC damage in these cases because fornix damage alone is sufficient to produce

anterograde amnesia[15]. A deficit in both verbal and visual recall has also been reported in patients who underwent callosotomy surgery for intractable epilepsy but only when the section included the posterior corpus callosum[16,17]. This is pertinent because the rostral splenium and posterior DHC fibers are intermingled, so split brain surgery involving the posterior corpus callosum always involves DHC transection.

The inferences we can derive from these small, methodologically heterogenous studies are, however, limited. Patients with verifiable DHC damage are extremely rare, and there are no reported cases of DHC damage sparing other relevant structures. An alternative approach is to examine whether inter-individual variation in the microstructure of the DHC is related to differences in memory performance. Begré et al., used diffusion tensor imaging (DTI) to search, voxel-wise, for a correlation between a measure of white matter microstructure (inter-voxel coherence) and performance in the Rey Visual Design Learning Test[18]. In their small sample (N=14), the authors reported that clusters of voxels demonstrating such a relationship overlapped with the DHC. The reported coordinates, however, correspond to the inferior-caudal surface of the splenium, whereas histological studies localise the DHC ventral to the corpus callosum body with posterior DHC fibers becoming intermingled with those of the *rostral* splenium[2]. The clusters reported by Begré et al., may therefore lack specificity to the DHC. Wei et al., recently demonstrated that white matter tractography and DW-MRI, can be used to isolate and reconstruct the trajectory of the human DHC, *in vivo*, but no individual subject-level reconstructions were shown (a group-level reconstruction was provided) and the study did not investigate the relationship between DHC microstructure and cognitive performance[19]. A study in a larger sample is therefore required to isolate the human DHC systematically and investigate the functional role of this tract in memory. Evidence that the DHC can be reconstructed accurately in nonhuman primates, where the tract morphology has been well characterised, would reinforce confidence in the accuracy of human DHC reconstructions.

104 In the present study, we report a semi-automated tractography approach that can be used to
105 reconstruct the DHC across humans (in vivo) and nonhuman primates (ex vivo). We also present tract
106 tracer findings highlighting that primate DHC fibers form a distinct tract and originate in the
107 parahippocampal region rather than the hippocampal formation. Finally, we derived diffusion tensor
108 imaging metrics from the DHC in a large sample of 100 human subjects, to investigate whether inter-
109 individual variation in the microstructure of this tract correlates with memory performance. We also
110 assessed whether the bilateral volumes of several relevant gray matter MTL regions relates to memory
111 performance.

112

113

114 **Results**

115 **Ex vivo non-human primate MR data**

116 To demonstrate the feasibility of a white matter tractography approach for investigating the role of
117 the DHC in human episodic memory, we first applied a multiple region-of-interest (ROI) deterministic
118 tractography protocol to diffusion- and T1-weighted images obtained from four ex vivo nonhuman
119 primate brain specimens (see Methods, Fig 1*A* and Fig 7). In all four specimens, this revealed a large
120 number of streamlines (mean: 2367.75, SD: 1383.791) that were broadly consistent with the known
121 anatomy of the non-human primate DHC (see Fig 1*B*-*E*). At the midline of the brain, the transverse
122 portion of the DHC streamlines was situated along the inferior aspect of the corpus callosum, just
123 anterior to the rostral splenium. More laterally, these streamlines arched inferiorly towards the
124 hippocampus and parahippocampal region. Whilst a number of these streamlines progressed
125 inferiorly towards regions along the parahippocampal gyrus (see Fig 1*A*, right), consistent with the
126 known anatomy, a number terminated in or around the hippocampus after having intersected our
127 hippocampal ROIs. This finding highlights limitations in resolving crossing fiber populations with

existing tractography techniques, and the fact that near the tail of the hippocampus, DHC fibers are known to merge with those of the fornix-fimbria and the alveus, which then cover the hippocampus[3]. Indeed, Fig 2*A*-*C* shows the DHC reconstruction for a representative specimen alongside streamlines corresponding to the fornix, which were reconstructed for illustrative purposes using a multiple-ROI approach reported previously[24]; whilst the transverse portion of the DHC is readily differentiated, more laterally, many of the DHC streamlines become intermingled with those of the fornix as the latter covers the hippocampus. Nevertheless, these ex vivo DHC reconstructions suggest that white matter tractography can be used to detect and reconstruct inter-hemispheric DHC connections, and that the transverse portion of these fiber pathway reconstructions in particular, is well characterised and differentiated from the fornix. The reconstructions were similar in humans (Fig 2*D*), so our subsequent quantitative analyses in human subjects were based on mean microstructure measures that were extracted from this transverse portion of the DHC (see Methods).

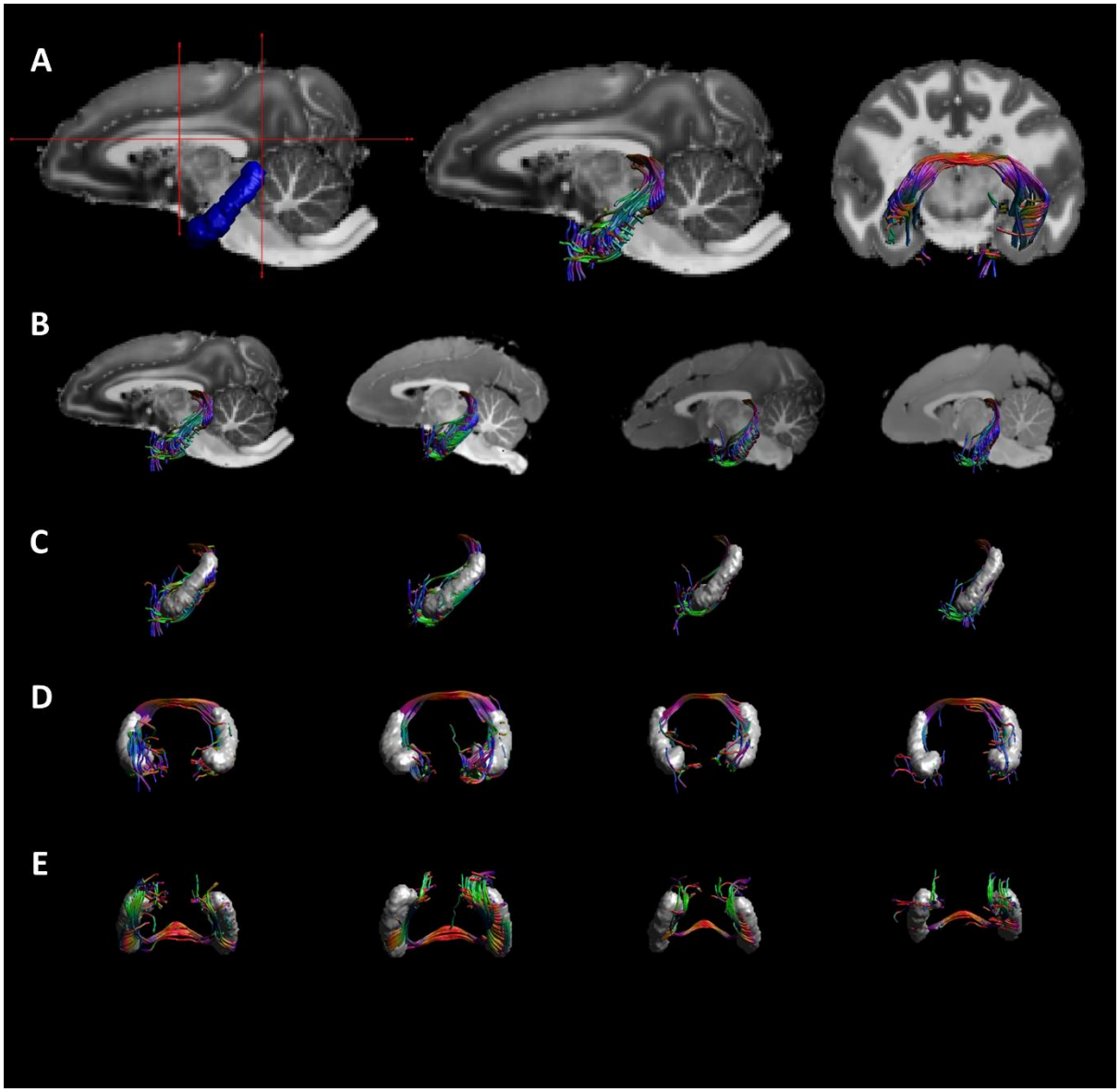

Figure 1. The hippocampal (blue) and manually-drawn (red lines) regions-of-interest (ROIs) used to extract the dorsal hippocampal commissure (DHC) in one representative specimen, and the subsequent reconstructions shown over a mid-sagittal and coronal section from the corresponding T1-weighted image in 0.5mm^3 native diffusion space (A); The reconstructions in all four specimens (B); The DHC reconstructions illustrated from a left-lateral, anterior-posterior, and inferior-superior perspective, alongside the anatomical hippocampal ROIs for spatial context (C, D and E, respectively). Note that for computational purposes, these renderings contain a 1/8th subsample of all reconstructed streamlines.

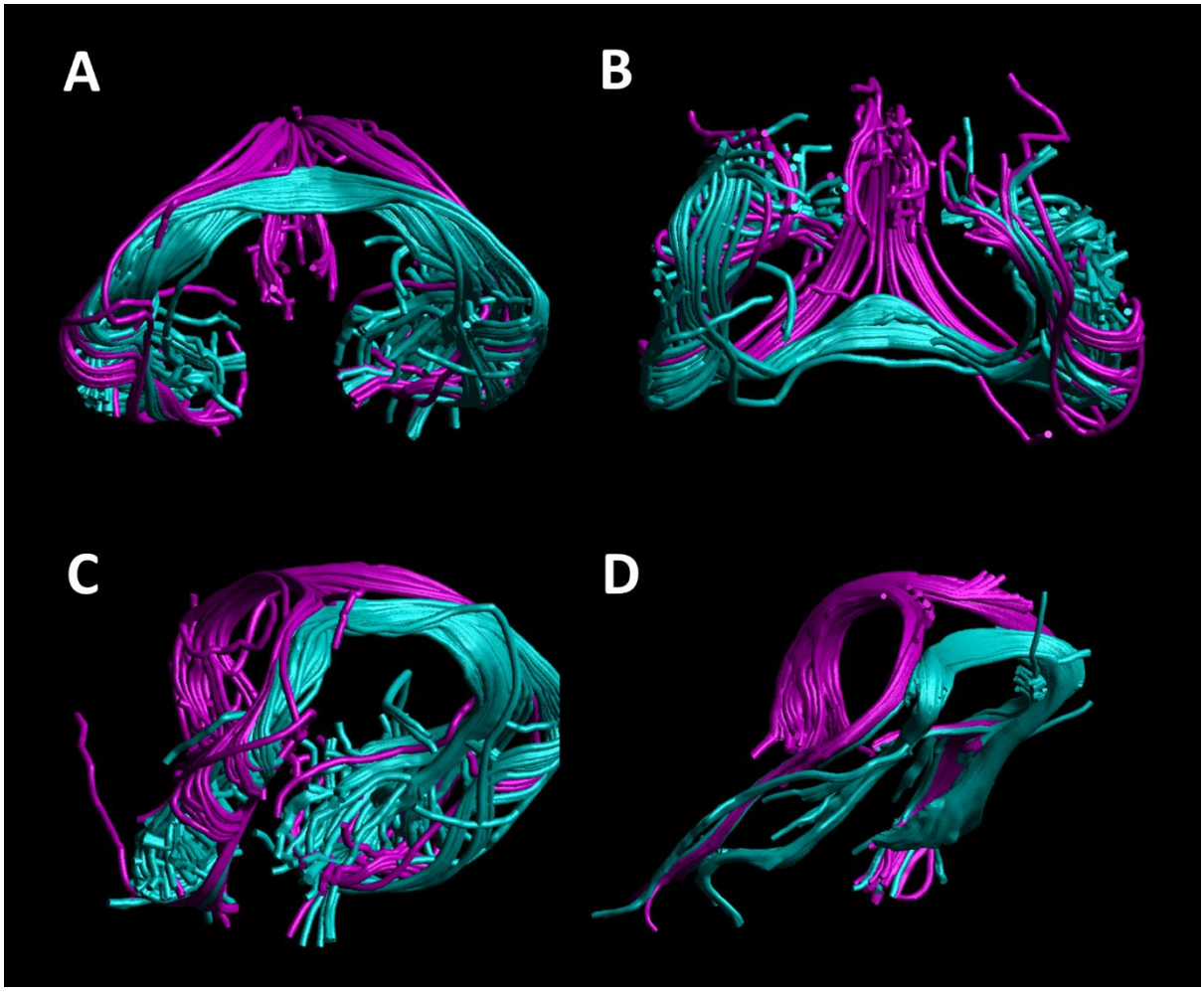

Figure 2. Dorsal hippocampal commissure (teal) and fornix (purple) streamlines reconstructed in a representative ex vivo nonhuman primate specimen, shown from a rear coronal-oblique (A), ventral (B) and left-lateral oblique (C) perspective. For comparison, streamlines corresponding to these two tracts are also shown for a representative Human Connectome Project (HCP) subject, from a left-lateral oblique perspective (D).

Ex vivo non-human primate tract tracer data

To highlight the veridical cortical origins of the inter-hemispheric DHC streamlines that were reconstructed in the previous analysis, we next examined bright- and dark-field photomicrographs taken from two ex vivo nonhuman primate specimens that had previously received anterograde tract tracer injections of radioactive amino acids in different locations within the medial temporal lobe. In

a specimen that received an injection in the hippocampal formation itself, centred on the subiculum, strong labelling was present in the ipsilateral but not the contralateral fornix or the DHC (Figs 3*A*-*C*). This is consistent with previous research showing that the majority of fibers comprising the fornix originate in the subicular cortices and CA subregions of the hippocampal formation, and that neither the fornix or DHC supports inter-hemispheric connections between these regions[25]. By contrast, dark field photomicrographs from a specimen that received an injection of tracer into caudal perirhinal and rostral parahippocampal cortex, revealed labelling in both the left and right DHC but almost no label in either the ipsilateral or contralateral fornix (Fig 3*D*-*E*). This distribution is consistent with DHC fibers originating in regions within the parahippocampal gyrus rather than the hippocampus proper. These findings highlight the distinct cortical origins of the nonhuman primate fornix and DHC.

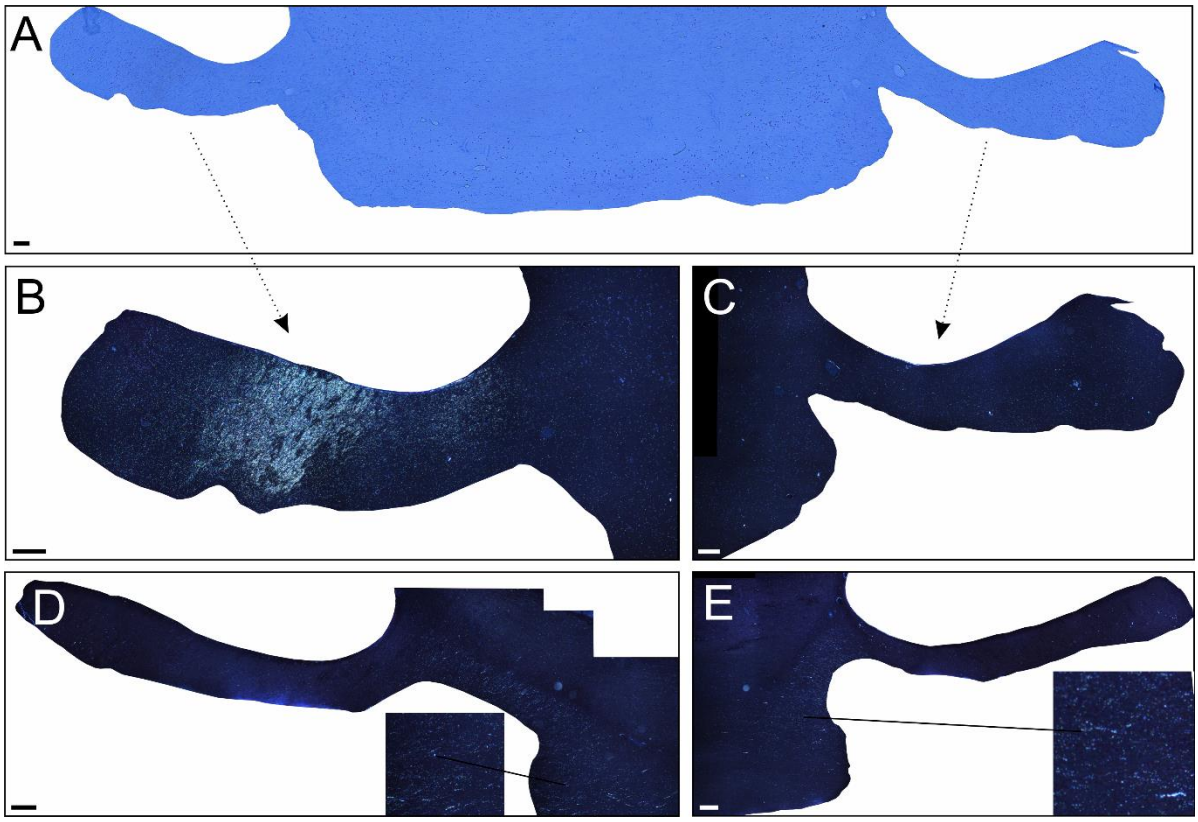

Figure 3. Bright- and dark-field photomicrographs of coronal sections taken at the level of the posterior fornix and dorsal hippocampal commissure (DHC), inferior to the corpus callosum. A) is a bright field photomicrograph from a case which received an anterograde tracer injection in the hippocampal formation centred in the

177 subiculum. B) and C) show dark field photomicrographs of the same section showing strong labelling in the
178 ipsilateral (B), but not contralateral (C), fornix; there was no obvious aggregation of label in the DHC. D) and E)
179 show dark field photomicrographs of a separate section from another case whose injection incorporated caudal
180 perirhinal and anterior parahippocampal cortex; these contain almost no label in the fornix but label in both the
181 left and right DHC. Magnified inserts are included in panels D-E to aid visibility of subtle DHC labelling in the
182 medial portion of the images. Scale bars = 200µm.

183

184

185 **In vivo human MR and cognitive data**

186 *Association between DHC microstructure and episodic memory performance*

187 We derived diffusion tensor imaging metrics (Fractional Anisotropy, FA, and Mean Diffusivity, MD[20])
188 from the DHC in a sub-sample of 100 participants in the Human Connectome Project (HCP) for whom
189 T1- and diffusion-weighted MRI data was available for analysis, along with performance in three
190 standardised memory tasks (the Picture Sequence Memory Test, PSMT[21]; List Sorting Working
191 Memory Test, LSWMT[22]; and Computerized Penn Word Memory task, CPWM[23]). This enabled us to
192 investigate whether inter-individual variation in DHC microstructure was correlated with memory
193 performance. For comparison, these analyses were repeated in another commissure tract – the AC
194 (see Methods).

195 Figure 4 illustrates the DHC reconstructions in four representative HCP subjects. Streamlines broadly
196 consistent with the known anatomy of the DHC were successfully reconstructed in 49 female and 47
197 male subjects (overall = 96%; females = 98%; males = 94%). Streamlines consistent with AC anatomy
198 were successfully reconstructed in 49 females and 50 males (overall = 99%; females = 98%; males =
199 100%). Measures of DHC and AC microstructure (FA and MD) are reported in Table 1. Independent
200 samples *t*-tests revealed higher DHC FA in females compared to males (t (94) = 2.852, p = 0.02, MD =
201 0.033, 95% CI = [0.01, 0.056]; d = 0.582). There were no other significant differences between males

202 and females in any of the microstructure metrics derived for either the DHC or AC (largest t (94) = -

203 1.853, p = 0.201, MD = -6.1 x 10^{-6}, 95% CI = [-126.8 x 10^{-6}, -4.4 x 10^{-6}], d = 0.372).

204

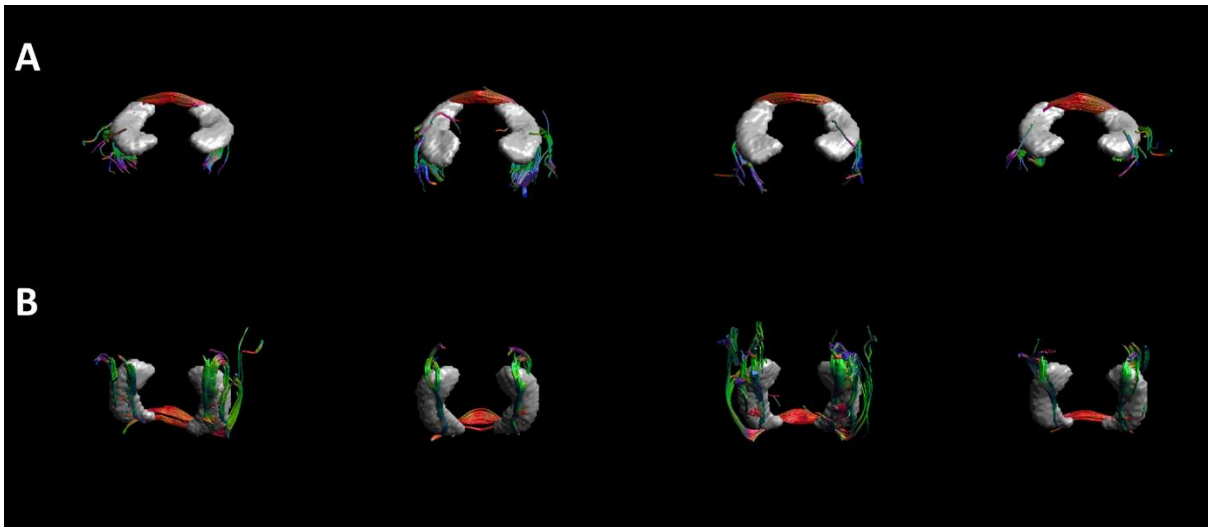

205

206 **Figure 4.** The dorsal hippocampal commissure reconstructions in four representative Human Connectome Project

207 datasets in the coronal (A) and axial (B) plane.

208

209 **Table 1.** Mean measures of DHC and AC microstructure in the HCP dataset (FA and MD) and N

210 streamlines reconstructed. Standard deviations are provided in brackets.

211

Tract	**Sample**	**Mean FA**	**Mean MD** (x10^{-3}mm^2 s^{-1})	**Mean N Streamlines**
DHC	All subjects	0.318 (0.059)	1.478 (0.163)	1622.47 (1981.16)
	Males	0.301 (0.061)	1.509 (0.184)	1354.75 (1920.46)
	Females	0.334 (0.052)	1.448 (0.137)	1879.27 (2023.91)
AC	All subjects	0.439 (0.05)	0.854 (0.051)	4102.68 (1896.59)

Males	0.435 (0.053)	0.862 (0.046)	4497.34 (2061.92)
Females	0.444 (0.046)	0.846 (0.055)	3699.96 (1635.87)

Cognitive performance in the CPWM, PSMT and LSWMT is reported in Table 2. Females typically scored higher than males on the CPWM task (t (98) = 3.120, p = 0.006, MD = 1.660, 95% CI = [0.604, 2.716], d = 0.624). There were no other significant gender differences in cognitive performance (largest t (98) = 2.082, p = 0.08, MD = 5.872, 95% CI = [0.274, 11.469], d = 0.416).

Table 2. Mean performance in the CPWM, PSMT and LSWMT. Raw scores are reported for the CPWM, and scaled scores are reported for the PSMT and LSWMT. Standard deviations are provided in brackets.

Sample	CPWM	PSMT	LSWMT
All subjects	35.79 (2.78)	112.15 (14.34)	110.15 (11.49)
Males	34.96 (3.04)	109.21 (13.72)	110.45 (10.77)
Females	36.62 (2.21)	115.09 (14.48)	109.84 (12.29)

A series of two-tailed Pearson correlation analyses revealed a significant negative association between MD and CPWM performance in the DHC (r = -0.269, p = 0.048, 95% CI = [-0.499, -0.017]), which was not evident in the AC (r = 0.100, p = 1.0, 95% CI = [-0.123, 0.297]); further, these correlations were significantly different from one another (Z = -2.608, p = 0.009, q = 0.376; see Fig 5). The correlations between DHC MD and both PSMT and LSWMT performance were not statistically significant (r = -

229 0.072, p = 1.0 , 95% CI = [-0.260, 0.096]; r = -0.047, p = 0.649, 95% CI = [-0.260, 0.159], respectively);
230 although they were not significantly different from the association between DHC MD and CPWM
231 performance (Z = -1.517, p = 0.065, q = 0.204; Z = -1.6, p = 0.055, q = 0.229, respectively). Across the
232 DHC and AC, there were no other statistically significant structure-cognition associations (largest r =
233 0.211, p = 0.240, 95% CI = [0.0, 0.403]). These findings imply a potential role for the DHC in CPWM
234 performance – a standardised episodic memory test.

235

236

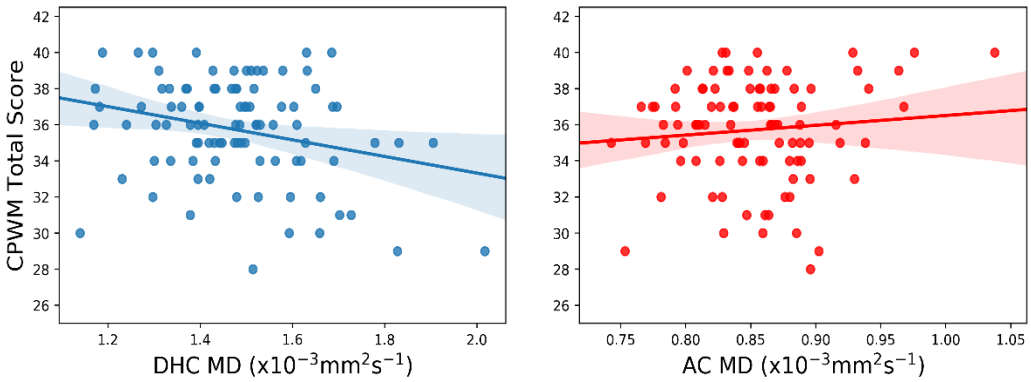

237

238 **Figure 5.** The correlation between white matter mean diffusivity (MD) and computerized Penn word memory
239 (CPWM) total scores in the dorsal hippocampal commissure (DHC; left) and anterior commissure (AC; right). The
240 best fitting linear regression line is plotted alongside 95% confidence intervals.

241

242 Given the statistically significant effect of gender upon several structural and cognitive measures, we
243 split the dataset and repeated these analyses separately for males and females. In the males, there
244 was again a negative association between DHC MD and CPWM performance, which was slightly
245 stronger than that observed in the whole sample but the association did not survive adjustment for
246 multiple comparisons (r = -0.290, p = 0.288, 95% CI = [-0.585, 0.022]). There were no other statistically

247 significant structure-cognition associations in either the DHC or AC for the male subjects (largest r =
248 0.216, p = 0.870, 95% CI = [-0.059, 0.458]).

249 Likewise, in the females, the negative association between DHC MD and CPWM performance was not
250 statistically significant (r = -0.116, p = 1.0, 95% CI = [-0.410, 0.183]). There was, however, a significant
251 positive relationship between AC MD and PSMT performance (r = 0.377, p = 0.048, 95% CI = [0.102,
252 0.572]), which was not recapitulated in the DHC (r = -0.173, p = 1.0, 95% CI = [-0.400, 0.063]); further,
253 these correlations were significantly different from one another (Z = 2.733, p = 0.006, q = 0.571; see
254 Fig 6). The corresponding associations between AC MD and performance in the CPWM and LSWMT
255 were not statistically significant (r = 0.268, p = 0.264, 95% CI = [-0.047, 0.504]; r = -0.047, p = 0.751,
256 95% CI = [-0.333, 0.276], respectively), and whilst the former was not significantly different to the
257 correlation between AC MD and PSMT performance (Z = 0.564, p = 0.286, q = 0.122), the latter was (Z
258 = 2.485, p = 0.006, q = 0.444). There were no further structure-cognition associations in the DHC or AC
259 that survived correction for multiple comparisons in the female subjects (largest r = -0.360, p = 0.06,
260 95% CI = [-0.581, 0.047]). These findings highlight a potential role for the AC in PSMT performance in
261 females.

262

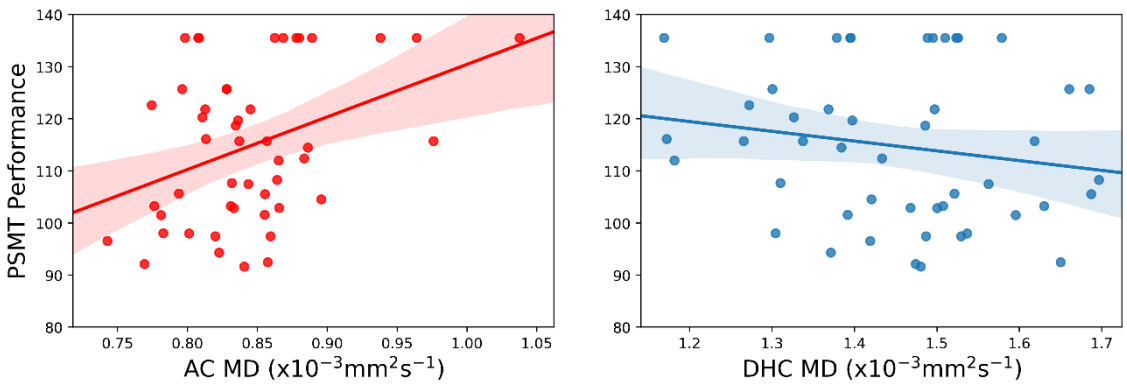

263

264 **Figure 6.** The correlation between white matter mean diffusivity (MD) and picture sequence memory task
265 (PSMT) performance in the anterior commissure (AC; left) and dorsal hippocampal commissure (DHC; right) in

the female HCP subjects reported here. The best fitting linear regression line is plotted alongside 95% confidence intervals and the data distribution for PSMT performance and MD in each tract.

Association between temporal regional volumes and memory

Using pre-existing regional volume estimates for our HCP sub-sample, we assessed whether the bilateral volumes of MTL gray matter regions including the hippocampus, amygdala, temporal pole, entorhinal and parahippocampal cortex, are also related to memory performance. These measures were first adjusted for differences in total Intra-Cranial Volume (ICV; see Methods), and are reported in Table 3. Independent samples pair-wise *t*-tests revealed no significant gender effect upon these ICV-adjusted bilateral volumes (largest t (98) = -1.294, p = 0.995, 95% CI = [-376.160, 79.232], d = 0.241). An independent samples *t*-test did, however, reveal a significant gender effect upon ICV itself, with larger ICVs for males compared to females (t (98) = -7.554, $p \leq 0.001$, MD = -213256.320, 95% CI = [-269276.819, -157235.82197], d = 1.511). Therefore, as well as adjusting our measures of gray matter volume for individual-differences in ICV across our entire HCP sub-sample, we also performed these adjustments separately for males and females for the purpose of subsequent correlational analyses that were split by gender. Following these gender-specific volumetric adjustments, the volumes of the hippocampi, amygdalae, parahippocampal cortex, entorhinal cortex and temporal pole were all larger in males compared to females (t (98) = -6.258, $p \leq 0.001$, MD = -832.980, 95% CI = [-1097.132, -568.828], d = 1.252; t (98) = -7.293, $p \leq 0.001$, MD = -450.240, 95% CI = [-572.758, -327.722], d = 1.459; t (98) = -4.502, $p \leq 0.001$, MD = -510.820, 95% CI = [-736.000, -285.640], d = 0.900; t (98) = -4.104, $p \leq 0.001$, MD = -428.640, 95% CI = [-635.912, -221.368], d = 0.821; t (98) = -2.430, p = 0.017, MD = -238.960, 95% CI = [-434.097, -43.823], d = 0.486, respectively).

290 **Table 3.** Mean ICV and ICV-adjusted volumes of bilateral temporal regions. Standard deviations are

291 provided in brackets.

292

Structure	Sample	Volume (mm^3)
Total ICV	All subjects	1587548.46 (176651.55)
	Males	1694176.62 (149159.31)
	Females	1480920.30 (132652.54)
Hippocampus	All subjects	8856.07 (663.78)
	Males	9272.56 (680.77)
	Females	8439.58 (649.97)
Amygdala	All subjects	3210.26 (310.89)
	Males	3435.38 (340.58)
	Females	2985.14 (273.10)
Entorhinal Cortex	All subjects	3460.21 (575.65)
	Males	3715.62 (637.70)
	Females	3204.80 (486.95)
Parahippocampal Cortex	All subjects	4391.78 (523.85)
	Males	4606.10 (509.48)
	Females	4177.46 (534.69)
Temporal Pole	All subjects	4682.52 (490.93)

	Males	4802.00 (469.73)
	Females	4563.04 (512.66)

There was no significant association between performance in any of the cognitive tasks (CPWM, PSMT, or LSWMT) and the bilateral ICV-adjusted volumes of these temporal regions (largest r = -0.189, p = 0.885, 95% CI = [-0.368, -0.004]). There were also no significant volume-cognition correlations when considering males and females separately (largest r in males = 0.312, p = 0.405, 95% CI = [0.058, 0.541]; largest r in females = -0.193, p = 1.0, 95% CI = [-0.406, 0.067]).

Discussion

This study demonstrated that white matter tractography can be used to reconstruct the DHC in both nonhuman primates (ex vivo) and humans (in vivo), and that these reconstructions broadly conform to the known anatomy of this understudied commissural fiber bundle. That these connections are distinct from those comprising the adjoining fornix is supported by the differential pattern of labelling observed in two ex vivo non-human primate specimens injected with anterograde radioactive tracer in either the subiculum of the hippocampal formation (dense labelling in the ipsilateral fornix) or perirhinal/parahippocampal cortex (labelling in the DHC). Inter-individual variation in the MD of the DHC reconstructions was also correlated with performance in a standardised episodic memory task – the CPWM. Importantly, this structure-cognition association was not evident in another commissural fiber bundle – the AC – implying a degree of specificity in the association between DHC microstructure and CPWM performance. In female subjects only, there was also evidence for a positive relationship between AC MD and PSMT performance, which was not recapitulated in the DHC, again implying

314 specificity in a role for the AC in PSMT performance. The bilateral volumes of several temporal gray
315 matter regions were not correlated with memory performance.

316 That our tractography approach affords reconstructions of the DHC across species is consistent with a
317 preservation of DHC morphology across humans and nonhuman primates[3]. Wei et al., recently showed
318 that a combination of manually and anatomically-defined ROIs, including the hippocampus, could be
319 used to reconstruct the human DHC in vivo[19]. Our findings augment those of Wei et al., by
320 demonstrating that this approach is reliable for large datasets, and by clearly defining a specific
321 combination of ROIs that yield DHC reconstructions that broadly reflect the known anatomy. The
322 transverse portion of the DHC reconstructions, in particular, is well differentiated from other local
323 fiber populations such as the fornix, and was therefore the focus of our subsequent quantitative
324 analyses.

325 The DHC is frequently described as a component of the fornix that supports inter-hemispheric
326 connections between the hippocampi [8,9]. Whilst consistent with the DHC reconstructions shown here,
327 this anatomical interpretation is potentially misleading. Our anterograde tract tracer data, for
328 instance, highlights the distinct hippocampal and parahippocampal origins of the fibers comprising the
329 fornix and DHC in nonhuman primates. The present specimens were previously reported alongside
330 others with more varied injections within the hippocampal formation; again, only in cases where
331 injections extended to parahippocampal regions was any incidental DHC labelling noted[25]. The cortical
332 origins of human DHC fibers have not been directly confirmed but the human DHC may also connect
333 parahippocampal regions rather than the hippocampi. Hippocampal ROIs can nevertheless be used to
334 seed DHC tractography, as evidenced by our tract reconstructions, because the hippocampus is
335 covered by the alveus and fimbria-fornix, which do themselves briefly merge with the DHC at the tail
336 of the hippocampus[3]. The successful propagation of DHC streamlines from hippocampal ROIs may
337 therefore reflect limitations in resolving crossing fiber populations that are associated with current
338 tractography techniques[26]. The same limitations result in a proportion of those streamlines also

339 terminating in the contralateral hippocampal ROIs, but several streamlines did nevertheless terminate
340 in contralateral parahippocampal regions. Although the DHC and fornix are partially contiguous, their
341 distinct cortical origins suggests that the former may play a unique – if complementary – role in
342 mnemonic processing.

343 We were limited to analysing cognitive data from the HCP cognitive task battery, which is not
344 necessarily optimised to investigate the role of the DHC in different memory processes. Interpretation
345 of the relationship between DHC MD and CPWM performance is therefore not straightforward. The
346 CPWM is an episodic memory task in which participants must discriminate between novel and pre-
347 exposed words, but participants are not required to perform free-recall of studied items. According to
348 dual-process models of recognition memory [5,27,28], performance in such tasks could be supported by a
349 *familiarity*-based recognition memory process, which is dependent on parahippocampal regions
350 within the MTL (particularly perirhinal cortex), rather than the hippocampus, which is instead critical
351 for successful performance in tasks that require conscious *recollection* (e.g., free recall). Our findings
352 therefore tentatively suggest that the DHC, may play a role in successful familiarity-based recognition
353 memory.

354 CPWM performance is not, however, a process-pure measure of familiarity-based recognition
355 memory. Although the CPWM places no explicit demands on recollection, this putatively distinct
356 mnemonic process may also be recruited to aid CPWM performance. Furthermore, the association
357 between DHC MD and CPWM performance was not significantly different to that between DHC MD
358 and PSMT performance, and successful performance in the latter task may be more dependent upon
359 recollection processes. To disentangle the specific memory processes that are partly dependent on
360 DHC connections, future studies should employ a variety of episodic memory paradigms that place
361 differential demands on familiarity and recollection-based recognition memory, including both free-
362 recall and forced-choice recognition tasks.

363 Whilst the CPWM employs verbal stimuli, the PSMT employs visual stimuli, albeit with additional
364 verbal descriptors. The present association between DHC MD and CPWM performance was not
365 significantly different to that between DHC MD and PSMT performance. Our study did not, therefore,
366 reveal a differential role for the DHC in verbal compared to visual memory. Future research should
367 employ matched verbal and visual memory paradigms to ascertain the extent to which inter-
368 hemispheric mnemonic processing of such stimuli depends upon DHC connections. A considerable
369 body of literature indicates a degree of hemispheric specialisation in visual and verbal processing[29–31].
370 Whilst we identified an association between DHC microstructure and performance in one verbal
371 episodic memory task, it is possible that DHC connections are particularly important for the mnemonic
372 processing of task-relevant conjunctions of visual and verbal information.

373 There were no significant correlations between measures of either DHC or AC microstructure and
374 performance in the LSWMT, implying that these tracts are not involved in working memory. However,
375 the correlations between DHC MD and a) CPWM performance and b) LSWMT performance, were not
376 statistically different. Future research should include tasks outside the episodic memory domain –
377 ensuring good variability in outcome measures – to assess any contribution of the DHC to other forms
378 of learning and memory. Our analyses also revealed no associations between memory measures and
379 the bilateral volumes of temporal regions that are known to be connected via the DHC/AC, or play a
380 role in successful recognition memory[4–7,32]. Further investigations are required to understand the
381 complex relationship between episodic memory performance, white matter microstructure and gray
382 matter macrostructure in this region.

383 When examining structure-cognition relationships that were significant at the group level, separately
384 by gender, the association between DHC MD and CPWM performance was stronger in males than
385 females, though it did not survive multiple comparison adjustment in either group. We also found a
386 significant and unexpected association between AC MD and PSMT performance in female subjects,
387 which was not evident in the males. The function of the AC is not well understood, but this finding

388 suggests a role for the AC in picture sequence recall in females, consistent with evidence that the AC
389 supports interhemispheric visual memory processing[33,34], and anecdotal reports of visual recall deficits
390 following AC damage[35]. These findings may also highlight distinct contributions of the DHC and AC to
391 episodic memory.

392 Additional gender effects included superior CPWM performance in females relative to males, which is
393 in line with previous reports[36]. Males typically had a larger ICV than females, and larger temporal
394 regional volumes when ICV adjustments were performed separately for these groups[37]. We observed
395 higher DHC FA in females relative to males but the evidence for gender-dependent differences in
396 white matter microstructure is equivocal; some studies show differences in several prominent tracts
397 but other studies show no differences in the same[38,39].

398 Our results imply that the human DHC is not vestigial, which has implications for the treatment of
399 several neurological conditions. The DHC could, for instance, be incorporated into models of the
400 cognitive impact of resective medial temporal lobe epilepsy surgeries[40,41]. Intracranial EEG studies
401 indicate that a subset of seizures with a medial temporal onset have a pattern of contralateral spread
402 to the hippocampus prior to involvement of contralateral neocortex, potentially via the DHC[3,42].
403 Indeed, whether due to bilateral hippocampal pathology or seizure spread, voxel-based morphometry
404 analyses have identified a cluster of voxels that incorporates the DHC, in which white matter volume
405 is reduced in temporal lobe epilepsy cases with bilateral hippocampal sclerosis compared to healthy
406 controls[43]. Our tractography protocols offer a complimentary approach to investigating whether DHC
407 microstructure is also compromised in epilepsy cases with mesial temporal sclerosis.

408 An advantage of our hypothesis-driven tractography approach, is that by constraining our analyses to
409 two commissural tracts, we reduce the risk of reporting both false-positive effects in regions for which
410 we have no specific predictions, and false-negative effects when true structure–cognition
411 relationships are obscured following corrections for large numbers of statistical comparisons. Another
412 advantage of our tractography approach, in which we extract DT-MRI-based microstructural indices

413 that are averaged over a given tract-of-interest, is that it may be more sensitive to subtle
414 microstructural differences that are distributed along the length of the tracts compared with voxel-
415 based methods in which such differences must be clustered in order to detect a significant effect in
416 group-level analyses (e.g., Tract-Based Spatial Statistics)[44]. Voxel-based methods and metrics that take
417 into account dispersed structural differences could, however, provide complimentary evidence of a
418 role for the DHC in memory. Anatomical Connectivity Mapping (ACM), has recently been proposed as
419 a method of quantifying the strength of connectivity of individual voxels with the rest of the brain[45].
420 Within a tract, the ACM metric at a given voxel may be sensitive to structural differences further along
421 that tract. Similar to our approach, an average or median ACM measure can also be derived for a given
422 tract-of-interest, and used in subsequent structure-behaviour or structure-cognition correlations[46].
423 ACM could potentially provide complimentary evidence of a role for the DHC in episodic memory.

424 Although DHC MD correlated with CPWM performance, DHC FA was not associated with performance.
425 FA and MD are both affected by multiple axonal properties, including myelination, density, diameter,
426 and configuration as well as partial volume interactions with tract size[26,47]. It is therefore not possible
427 to attribute differences between our FA/MD findings to a single white-matter subcomponent.

428 In summary, to our knowledge this is the first study to use cross-species anatomical evidence to
429 highlight the DHC as a discrete tract in primates and to systematically reconstruct it using advanced
430 tractography techniques. Reconstructions of the human and nonhuman primate DHC broadly conform
431 to the known anatomy of this tract, affording investigations of the role of the DHC in learning and
432 memory. Indeed, we are also the first to demonstrate a correlation between inter-individual variation
433 in the microstructure of *in vivo* DHC tract reconstructions and differences in a measure of episodic
434 memory performance. Our understanding of the unique role of the DHC in human learning and
435 memory, in both health and disease, is sparse, but the approach described here should advance our
436 knowledge of those aspects of human memory that are partly dependent upon inter-hemispheric
437 processing via the DHC.

438

439 **Methods**

440 ***Data***

441 *Ex vivo non-human primate MR data*

442 Diffusion- and T1-weighted MR data that were obtained previously from the perfusion-fixed brains of
443 four healthy adult female vervet monkeys (*Chlorocebus sabeus;* specimens e3429, e3487, e3494, and
444 e4271), were available for analysis (age range = 32-48 months; mean = 36.25, SD = 7.85). The animals
445 were obtained from the Behavioral Science Foundation, St. Kitts and were socially housed in enriched
446 environments. The experimental procedures were reviewed and approved by the Institutional Review
447 Board of the Behavioral Science Foundation, acting under the auspices of the Canadian Council on
448 Animal Care. The postmortem brains were prepared for data collection on a preclinical 4.7 T Agilent
449 scanner system at the Danish Research Centre for Magnetic Resonance using an *ex vivo* imaging
450 protocol reported previously[48,49]. This included a DW-MRI pre-scan of at least 15 hours duration to
451 avoid introducing short-term instabilities into the final DW-MRI datasets (e.g., due to motion caused
452 by physical handling of the tissue[48,50]). The brain specimens were also stabilized to room temperature
453 prior to scanning, and a conditioned flow of air around the specimen was maintained throughout
454 scanning to reduce temperature drifts of the diffusion signal[48,50].

455 Diffusion-weighted images were collected using a diffusion-weighted pulsed gradient spin echo
456 sequence with single line readout. The scan parameters were as follows: repetition time, TR = 7200
457 (but TR = 8400ms for subject e4271); echo time, TE = 35.9ms; gradient separation, DELTA = 17.0ms;
458 gradient duration, delta = 10.5ms; gradient strength, g = 300 mT/m; number of repetitions, NEX = 2
459 (averaged offline); matrix size = 128 x 256 with 100 axial slices offering whole brain coverage with
460 isotropic 0.5mm voxels. Gradients were applied along 68 uniformly distributed directions with a b-
461 value of 9686 s/mm^2 using scheme files available from the Camino tool kit[51]. Thirteen non diffusion-

weighted images with b = 0 s/mm^2 were also acquired. T1-weighted images were acquired using a 3D MPRAGE sequence with 0.27mm isotropic voxels and the following parameters: TR = 4ms; TE = 2ms; TI = 800ms; FA = 9°; matrix = 256 x 256 x 256, axial image plane.

Ex vivo non-human primate anterograde tract tracer data

To highlight the distinct origins of fibers comprising the DHC and the nearby fornix, we examined ex vivo brain specimens obtained from two male cynomolgus monkeys (*Macaca fascicularis* - ACy14 and ACyF23) aged 1-2 years, that had received anterograde tract tracer injections in different medial temporal lobe regions for a previous study of the origin and topography of the fibers comprising the fornix[25]. Like the vervet monkeys used for our ex vivo tractography analyses, cynomolgus monkeys are members of the *Cercopithecinae* subfamily of Old World monkeys, and the anatomy of the brain is considered to be very similar across these species[52]. The reader is referred to the original manuscript for a detailed description of the stereotactic surgery and subsequent brain extraction protocols[25], but briefly, a cocktail of tritiated amino acids was injected into distinct target regions within the medial temporal lobe across the two cases. This cocktail was composed of an equal-parts mixture of either tritiated proline and leucine (final concentration of 50 µCi/µl, New England Nuclear), or tritiated proline, leucine, lysine, and an amino acid mixture derived from algal protein hydrosylate (final concentration of 100 µCi/µl, New England Nuclear), and was injected into the surgically exposed target region using a Hamilton syringe. Specimen ACy14 received an injection in the hippocampal formation, centred in the subiculum, whereas specimen ACyF23 received an injection that incorporated the caudal perirhinal cortex and the rostral parahippocampal cortex. Following a 5-10 day postoperative survival period, the two monkeys were deeply anesthetized and the brain was extracted and cryoprotected. The specimens were cut into 33µm coronal sections, coated with emulsion and subsequently exposed at 4 ^{0}C for 6-30 weeks before being developed and counterstained for thionine. Specimen ACyF23 had undergone a bilateral fornix transection procedure 2-12 months prior to the

injection of the tritiated amino acids; the case is nevertheless informative because the subsequent amino acid injections resulted in labelling up to the point of the transection.

In vivo human MR and cognitive data

Cognitive, diffusion- and T1-weighted MR data were obtained for 100 subjects from the Q3 release of the Human Connectome Project (50 males, aged 22-35 years)[53–55]. The participants in that previous study were recruited from Washington University and the surrounding area and gave informed consent in line with policies approved by the Washington University Institutional Review Board.We co-opted these data for the present analyses to exploit the high-quality diffusion-weighted images that are acquired through the HCP owing to the superior gradient strengths afforded by their customized gradient set. This subsample of the available HCP data will henceforth be referred to as the 'HCP dataset'.

For each subject, whole-brain diffusion- and T1-weighted images had been acquired on a customized 3T Connectom Skyra scanner (Siemens, Erlangen) with a 32-channel head coil and a customised SC72C gradient set. Each pre-processed dataset comprised 90 diffusion directions for each of three shells with *b*-values of 1000, 2000 and 3000 s/mm^2; these images were acquired with TR = 5500ms, TE = 89ms and 1.25mm^3 isotropic voxels. 18 images with b = 0 s/mm^2 were also acquired. Corresponding T1-weighted images were acquired by taking two averages using the 3D MPRAGE sequence [56], with 0.7mm^3 isotropic voxels and the following parameters: TR = 2400ms, TE = 2.14ms, TI = 1000ms, FA = 8°, FOV = 224mm, matrix = 320 x 320 x 256 sagittal slices in a single slab. Note that the pre-processed HCP diffusion datasets are aligned to the T1 images using FLIRT[57,58] as standard so that both the diffusion and T1 data that were available to us were pre-aligned in 1.25mm native structural space. Further acquisition parameters and details of the minimal MR pre-processing pipeline have been reported previously[53,54].

511 Available cognitive data for the HCP subjects included performance in the Computerized Penn Word
512 Memory task (CPWM)[23], the Picture Sequence Memory Test (PSMT)[21] and the List Sorting Working
513 Memory Test (LSWMT)[22]. The CPWM is a verbal episodic memory task in which a participant is
514 required to discriminate 20 pre-exposed target word stimuli from 20 inter-mixed novel distractor
515 stimuli; performance is quantified here as subjects' total number of correct responses. In the PSMT,
516 another episodic memory task, subjects are required to learn and recall a sequence of picture stimuli
517 over a number of trials and performance is scored as the cumulative number of adjacent pairs of
518 pictures that are correctly recalled over 3 learning trials. In the LSWMT, subjects are presented with a
519 series of picture stimuli on a computer screen (e.g., an elephant and a mouse) and are required to
520 remember the stimuli comprising the sequence, mentally reorder them from smallest to largest, and
521 finally recite the revised sequence of stimuli; performance is scored as the number of correct
522 responses across the stimulus lists that comprise this working memory task. For both the PSMT and
523 LSWMT, HCP subjects' raw scores have been standardised against the NIH Toolbox normative
524 sample[59]. These standardised scores can also be age-adjusted, but given that we had non age-adjusted
525 raw scores for the CPWM, we used subjects' unadjusted PSMT and LSWMT scores for subsequent
526 analyses.

527 Finally, pre-existing regional volume measures were available for a number of relevant cortical and
528 subcortical regions in the HCP dataset, because the T1- and T2- weighted images that are acquired for
529 the HCP are segmented using Freesurfer software as part of the standard pre-processing pipeline[53].
530 We used these data to investigate whether differences in CPWM, PSMT and/or LSWMT performance,
531 are also related to the volume of several key gray matter regions within the MTL. Our specific regions-
532 of-interest (ROIs) were the hippocampi, amygdalae, entorhinal cortex, parahippocampal cortex (areas
533 TH and TF), as well as the temporal pole, and estimates of total Intracranial Volume (ICV). The
534 hippocampus was of interest because the DHC is sometimes assumed to support dense inter-
535 hippocampal connections, despite an absence of confirmatory evidence[2]. By contrast, the entorhinal
536 and parahippocampal cortices are known to project to contralateral structures via the DHC[1,2], and they

537 also provide a functionally important input/output pathway for the hippocampus itself[4]. The temporal
538 pole and amygdala were ROIs that are known to project to or receive from contralateral structures via
539 the anterior commissure (AC), which was used as a comparison tract for our tractography analyses, as
540 described below[1,60,61].

541

542

543 **Data Processing**

544 *Ex vivo non-human primate MR data*

545 The T1-weighted images for each nonhuman primate specimen were masked to contain only brain
546 tissue using FSL utilities[62]. Gray/white matter contrast is reversed in our T1 images of *ex vivo* tissue[63];
547 we therefore inverted the T1-weighted images for subsequent processing and display purposes. The
548 T1-weighted brain images were then submitted to the standard Nonhuman Primate EMSegmenter
549 pipeline in 3DSlicer version 4.9.0. The pipeline registers the T1-weighted image to a probabilistic
550 vervet monkey MRI atlas using BRAINSFit[64,65], and segments the image into unilateral ROIs, including
551 the hippocampus, using the EM segmenter algorithm[66]. The subject-specific aligned and unbiased
552 hippocampus segmentations were thresholded at 40%, binarised, and brought into native diffusion
553 space using FLIRT, ready for use as ROIs for tractography.

554 Visual inspection of the DW-MRI datasets revealed that no additional pre-processing was required to
555 adjust for motion or eddy currents prior to streamline reconstruction[49]. A multiple-ROI tractography
556 approach (see Fig 7*A*) was used to reconstruct the DHC. Tractography was performed from all voxels
557 in the left hippocampus ROI in subjects' native diffusion-space in ExploreDTI v4.8.3[67]using a
558 deterministic tractography algorithm based on constrained spherical deconvolution[68,69]. The
559 contralateral hippocampal ROI was used as an 'AND' gate to capture any propagated streamlines that
560 terminated in the contralateral hippocampal/parahippocampal region. Three additional 'NOT' ROIs

were manually drawn to exclude streamlines corresponding to other pathways. These included: 1) An ROI covering the entire section, drawn on the most inferior axial slice where the body of the corpus callosum was visible, 2) A coronal ROI covering the entire section placed at a slice where the parahippocampal cingulum begins to descend behind the splenium, and 3) A coronal ROI covering the entire section except the temporal lobes, placed at the slice where the anterior fornix columns descend towards the mammillary bodies. Additional exclusionary ROIs were used to remove extant spurious streamlines as required. A step size of 0.1mm and an angle threshold of 60 degrees was applied to prevent the reconstruction of anatomically implausible streamlines. Tracking was performed with a supersampling factor of 4 x 4 x 4, so that streamlines were initiated from 64 grid points, uniformly distributed within each voxel.

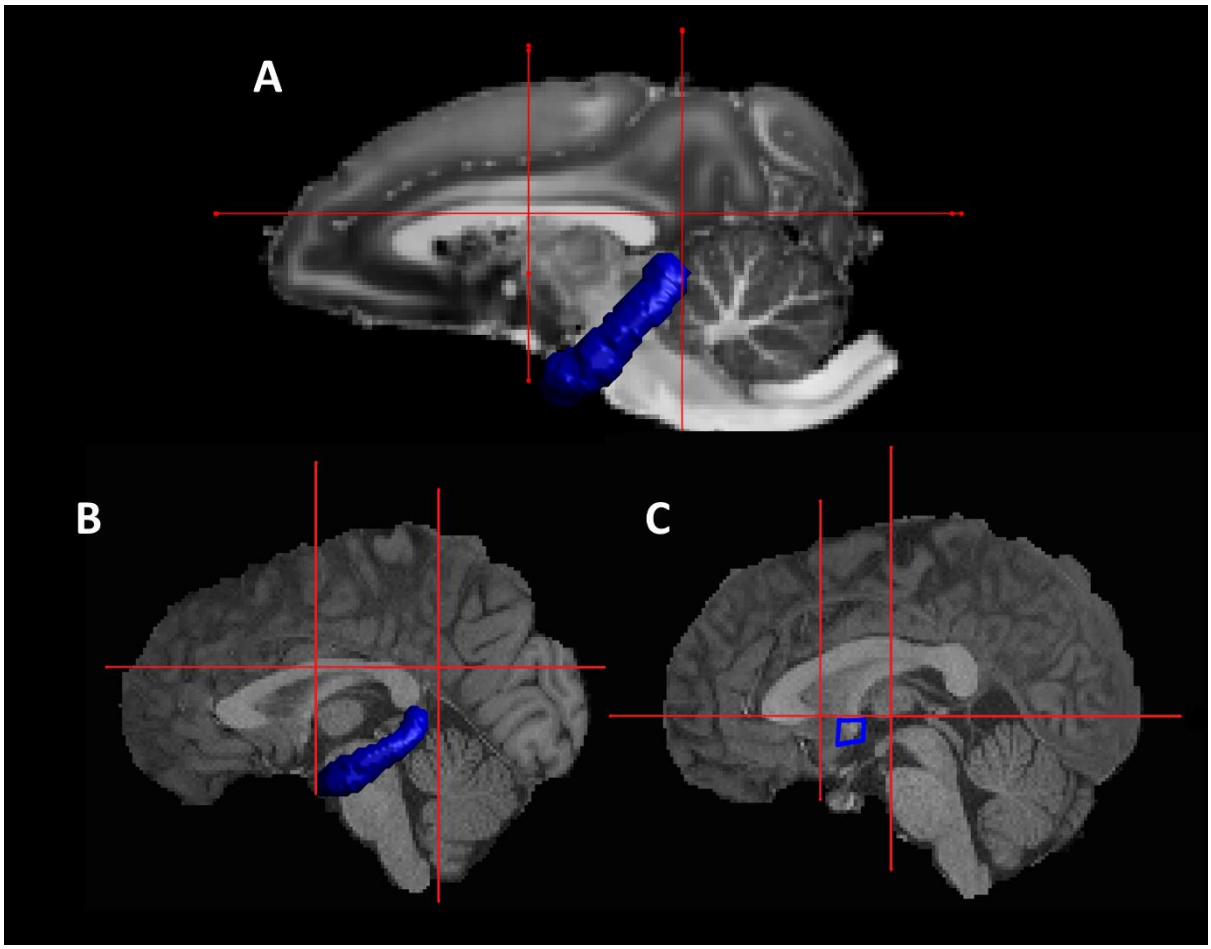

573

574 **Figure 7.** The hippocampal (blue) and manually drawn (red lines) regions-of-interest (ROIs) used for dorsal
575 hippocampal commissure tractography shown on a mid-sagittal section of a T1-weighted image for a
576 representative ex vivo nonhuman primate specimen in 0.5mm^3 native diffusion space (A) and a Human
577 Connectome Project (HCP) subject in 1.25mm^3 native diffusion space (B). Also shown are the manually-drawn
578 ROIs used for anterior commissure tractography (red and yellow lines) in a representative HCP subject (C).

579

580 *Ex vivo non-human primate anterograde tract tracer data*

581 A Leica DM500B microscope with a Leica DFC310FX digital camera and Leica Application Suite v4.7
582 image acquisition software were used to obtain both bright- and dark-field images from our ex vivo
583 cynomolgus monkey specimens.

584

585 *In vivo human MR and cognitive data*

586 Whole brain voxel-wise maps of two DTI measures of white matter microstructure – Fractional
587 Anisotropy and Mean Diffusivity (FA and MD, respectively)[20] - were derived from the b = 1000 s/mm^2
588 images. Unilateral hippocampal ROIs were segmented from subjects' T1-weighted images using
589 FIRST[70]. Streamlines were then seeded from the left hippocampus using the same combination of ROIs
590 described above (Fig 7*B*), and a multi-shell multi-tissue constrained spherical deconvolution algorithm
591 (MSMT-CSD) was applied to the subjects' complete diffusion dataset[71]. This process was then repeated
592 with tractography seeded from the right hippocampus. Tracking parameters were the same as above
593 except a step size of 0.5 mm was applied. Two additional ROIs were then drawn around the DHC
594 reconstructions on sagittal sections located 5 slices from the midline of the brain to extract a
595 transverse segment of the DHC, where the streamlines are well differentiated from those of other
596 local white matter pathways. This was done separately for the reconstructions obtained by seeding

tractography from the left and right hemispheres. The transverse DHC segments were intersected with the whole brain voxel-wise FA and MD maps. For both FA and MD, the mean measures obtained from the two segments were then combined into a vertex-weighted mean measure as follows:

$$\text{Vertex-Weighted Mean FA} = \frac{(N_{L\rightarrow R} \times \overline{FA_{L\rightarrow R}}) + (N_{R\rightarrow L} \times \overline{FA_{R\rightarrow L}})}{(N_{L\rightarrow R} + N_{R\rightarrow L})}$$

$$\text{Vertex-Weighted Mean MD} = \frac{(N_{L\rightarrow R} \times \overline{MD_{L\rightarrow R}}) + (N_{R\rightarrow L} \times \overline{MD_{R\rightarrow L}})}{(N_{L\rightarrow R} + N_{R\rightarrow L})}$$

where $N_{L\rightarrow R}$ and $N_{R\rightarrow L}$ refer to the number of vertices comprising the tract segment obtained by seeding tractography from the left and right hemisphere, respectively. $\overline{FA_{L\rightarrow R}}$ and $\overline{FA_{R\rightarrow L}}$ refer to the mean FA measure obtained from the left- and right-seeded segment; likewise, $\overline{MD_{L\rightarrow R}}$ and $\overline{MD_{R\rightarrow L}}$ refer to the mean MD measure obtained from the left- and right-seeded segment. These vertex-weighted measures of mean FA and MD take into account any potential differences in the number of streamlines that comprise the left versus right-seeded segments, and were later correlated with memory measures. For the sake of brevity, in the remainder of the text we refer simply to mean FA and MD measures without reference to the vertex-weighting that was applied.

For comparison, these measures were also obtained from a transverse segment of the anterior commissure (AC). The AC is a commissural fiber pathway – the function of which is not well understood – that provides interhemispheric connections between the temporal pole, the amygdala, the superior and inferior temporal gyri, and the parahippocampal gyrus[2]. Given that both the DHC and AC contain fibers that originate and cross in the parahippocampal gyrus, we restricted our AC analyses to those

621 relatively 'anterior projections' of this fiber bundle, which involve the temporal pole and amygdala.
622 This was achieved by seeding tractography from an ROI manually drawn around the AC on a sagittal
623 section 5 slices from the midline, where the AC is visible at the point it bifurcates the descending fornix
624 columns (see Fig 7*C*). This 'SEED' ROI was initially drawn in the left hemisphere, and a corresponding
625 'AND' ROI was placed at the same point in the right hemisphere. An exclusionary 'NOT' ROI with
626 whole-brain coverage was then drawn on an axial slice immediately above the AC. Another, covering
627 the whole brain except the temporal lobes, was drawn on a coronal section immediately posterior to
628 the rostrum of the corpus callosum. A final 'NOT' ROI was drawn around the whole brain on a coronal
629 section located just anterior to the pons. This procedure was repeated with the seed and the AND
630 ROIs placed in the opposite hemispheres. The initial seed and 'AND' ROIs were then used to extract a
631 transverse segment of the AC from both reconstructions. Mean FA and MD metrics were extracted
632 and combined using the above formula.

633

634 *Statistical Analysis*

635 Two-tailed Pearson correlation statistics were used to investigate the relationship between DT-MRI
636 measures of DHC and AC microstructure (FA and MD), and performance in three standardised memory
637 tasks (CPWM, PSMT and LSWMT). Correlation statistics were computed with 1000 bootstrapped
638 samples to derive 95% confidence intervals, and a Bonferonni-Holm step-down procedure was used
639 to adjust derived *p*-values for six structure-cognition correlations, separately for each tract (the DHC
640 and AC). Subjects in whom both the DHC and AC were successfully reconstructed were included in
641 these analyses to enable fair comparisons between dependent correlations across these tracts. To test
642 for differences between correlations across the DHC and AC, any significant structure-cognition
643 associations identified in one tract, were compared with the corresponding correlation in the other
644 tract using one-tailed Steiger Z tests, which are reported alongside Cohen's *q* effect size measures[72].
645 A significance threshold of $p = 0.05$ was used for all comparisons.

646 The same correlational approach was used to investigate the relationship between memory
647 performance (in the CPWM, PSMT and LSWMT) and the volume of individual temporal lobe regions
648 including the amygdala, hippocampus, temporal pole, entorhinal and parahippocampal cortices.
649 Bilateral volume measurements were used to maximise statistical power, and *p*-values were
650 Bonferonni-Holm adjusted for fifteen volume-cognition correlations. Regional gray matter volume
651 measures are often confounded by inter-individual differences in total intracranial volume (ICV); we
652 therefore used the following formula to adjust volume measurements for differences in ICV prior to
653 any correlational analyses:

654

655 $$Measure_{adjusted} = Measure_{raw} - \beta\ (ICV_{raw} - ICV_{mean})$$

656

657 where ICV_{raw} refers to a subject's ICV estimate, ICV_{mean} refers to the mean ICV in the HCP dataset, and
658 β refers to the slope of the regression line between ICV and the measure of interest[73].

659 Given previous evidence of gender effects upon white matter microstructure, gray matter
660 macrostructure and cognition[74–76], we also used two-tailed independent samples *t*-tests and Cohen's
661 *d* effect size measures[72] to investigate whether there was a potential effect of gender upon our
662 microstructure, macrostructure or cognitive measures. Where gender effects were evident, the above
663 analyses were repeated separately for males and females.

664

665 **Acknowledgements**

666 DKJ and GDP are supported by a Wellcome Trust Investigator Award (096646/Z/11/Z) and a Wellcome
667 Trust Strategic Award (104943/Z/14/Z). MP* is currently supported by the Medical Research Council
668 (MR/N01233X/1). Data used in the preparation of this work were obtained from the MGH-USC Human
669 Connectome Project (HCP) database (https://ida.loni.usc.edu/login.jsp). The HCP project (Principal

Investigators: Bruce Rosen, M.D., Ph.D., Martinos Center at Massachusetts General Hospital; Arthur W. Toga, Ph.D., University of California, Los Angeles, Van J. Weeden, MD, Martinos Center at Massachusetts General Hospital) is supported by the National Institute of Dental and Craniofacial Research (NIDCR), the National Institute of Mental Health (NIMH) and the National Institute of Neurological Disorders and Stroke (NINDS). Collectively, the HCP is the result of efforts of co-investigators from the University of California, Los Angeles, Martinos Center for Biomedical Imaging at Massachusetts General Hospital (MGH), Washington University, and the University of Minnesota.

Author Contributions

MW developed the initial concept for this study, and the subsequent study design was developed by MP*, DKJ, and MW. Ex vivo vervet monkey MR images were previously acquired by HL, MP, and TBD, who contributed these existing datasets for the present tractography analyses. JA obtained and contributed both bright and dark field images from existing ex vivo cynomolgus monkey specimens. MP*, and MW performed tractography analyses with input from GDP, and under the supervision of DKJ. All statistical analyses were performed by MP* and MW with input from DKJ. All authors provided critical revision of the manuscript, thereby providing important intellectual content.

Competing Interests Statement

The authors declare no competing interests.

Data Availability

The nonhuman primate MR data that support the findings of this study are available from the Danish Research Centre for Magnetic Resonance but restrictions apply to the availability of these data, which were used under written agreement for the current study, and so are not publicly available. Derived data are, however, available from the corresponding author.

All photomicrographs of nonhuman primate specimens that were generated for this study are available in the manuscript.

The human MRI and cognitive test data that support the findings of this study are available under license from the Human Connectome Project (https://db.humanconnectome.org/); derived data are also available from the corresponding author upon reasonable request.

References

1. Demeter, S., Rosene, D. L. & van Hoesen, G. W. Interhemispheric pathways of the hippocampal formation, presubiculum, and entorhinal and posterior parahippocampal cortices in the rhesus monkey: The structure and organization of the hippocampal commissures. *J. Comp. Neurol.* **233,** 30–47 (1985).

2. Demeter, S., Rosene, D. L. & Van Hoesen, G. W. Fields of origin and pathways of the interhemispheric commissures in the temporal lobe of macaques. *J. Comp. Neurol.* **302,** 29–53 (1990).

3. Gloor, P., Salanova, V., Olivier, A. & Quesney, L. F. The human dorsal hippocampal commissure. *Brain* **116,** 1249–1273 (1993).

4. Aggleton, J. P. Multiple anatomical systems embedded within the primate medial temporal lobe: Implications for hippocampal function. *Neurosci. Biobehav. Rev.* **36,** 1579–1596 (2012).

716 5. Aggleton, J. P. & Brown, M. W. Episodic memory, amnesia, and the hippocampal-anterior
717 thalamic axis. *Behav. Brain Sci.* **22,** 425-444; discussion 444-489 (1999).

718 6. Squire, L. R. & Zola-Morgan, S. The medial temporal lobe memory system. *Science* **253,** 1380–
719 1386 (1991).

720 7. Zola-Morgan, S., Squire, L. R., Amaral, D. G. & Suzuki, W. A. Lesions of perirhinal and
721 parahippocampal cortex that spare the amygdala and hippocampal formation produce severe
722 memory impairment. *J. Neurosci.* **9,** 4355–4370 (1989).

723 8. Raslau, F. D. *et al.* Memory part 3: The role of the fornix and clinical cases. *Am. J. Neuroradiol.*
724 **36,** 1604–1608 (2015).

725 9. Tubbs, R. S. *et al.* The Enigmatic Psalterium: A Review and Anatomic Study With Relevance to
726 Callosotomy Procedures. *Oper. Neurosurg.* **11,** 322–328 (2015).

727 10. Mark, L. P., Daniels, D. L., Naidich, T. P., Yetkin, Z. & Borne, J. a. Anatomic moment - the
728 hippocampus. *Am. J. Neuroradiol.* **14,** 709–712 (1993).

729 11. Moss, M., Mahut, H. & Zola-Morgan, S. Concurrent discrimination learning of monkeys after
730 hippocampal, entorhinal, or fornix lesions. *J. Neurosci.* **1,** 227–240 (1981).

731 12. Mahut, H., Moss, M. & Zola-Morgan, S. Retention deficits after combined amygdalo-
732 hippocampal and selective hippocampal resections in the monkey. *Neuropsychologia* **19,**
733 201–225 (1981).

734 13. Heilman, K. M. & Sypert, G. W. Korsakoff's syndrome resulting from bilateral fornix lesions.
735 *Neurology* **27,** 490 LP-490 (1977).

736 14. D'Esposito, M., Verfaellie, M., Alexander, M. P. & Katz, D. I. Amnesia following traumatic
737 bilateral fornix transection. *Neurology* **45,** 1546–1550 (1995).

738 15. Aggleton, J. P. EPS Mid-Career Award 2006. Understanding anterograde amnesia:

739 disconnections and hidden lesions. *Q. J. Exp. Psychol. (Hove).* **61,** 1441–1471 (2008).

740 16. Phelps, E. A., Hirst, W. & Gazzaniga, M. S. Deficits in recall following partial and complete
741 commissurotomy. *Cereb. Cortex* **1,** 492–491 (1991).

742 17. Clark, C. R. & Geffen, G. M. Corpus callosum surgery and recent memory: A review. *Brain* **112,**
743 165–175 (1989).

744 18. Begré, S., Kiefer, C., Von Känel, R., Frommer, A. & Federspiel, A. Rey Visual Design Learning
745 Test performance correlates with white matter structure. *Acta Neuropsychiatr.* **21,** 67–74
746 (2009).

747 19. Wei, P. H. *et al.* In vivo visualization of connections among revised Papez circuit hubs using
748 full q-space diffusion spectrum imaging tractography. *Neuroscience* **357,** 400–410 (2017).

749 20. Basser, P. J. & Pierpaoli, C. Microstructural and physiological features of tissues elucidated by
750 quantitative-diffusion-tensor MRI. *J. Magn. Reson.* **213,** 560–570 (2011).

751 21. Dikmen, S. S. *et al.* Measuring episodic memory across the lifespan: NIH toolbox picture
752 sequence memory test. *J. Int. Neuropsychol. Soc.* **20,** 611–619 (2014).

753 22. Tulsky, D. S. *et al.* NIH toolbox cognition battery (NIHTB-CB): List sorting test to measure
754 working memory. *J. Int. Neuropsychol. Soc.* **20,** 599–610 (2014).

755 23. Moore, T. M., Reise, S. P., Gur, R. E., Hakonarson, H. & Gur, R. C. Psychometric properties of
756 the Penn Computerized Neurocognitive Battery. *Neuropsychology* **29,** 235–246 (2015).

757 24. Metzler-Baddeley, C., Jones, D. K., Belaroussi, B., Aggleton, J. P. & O'Sullivan, M. J.
758 Frontotemporal connections in episodic memory and aging: a diffusion MRI tractography
759 study. *J. Neurosci.* **31,** 13236–13245 (2011).

760 25. Saunders, R. C. & Aggleton, J. P. Origin and topography of fibers contributing to the fornix in
761 macaque monkeys. *Hippocampus* **17,** 396–411 (2007).

762 26. Jones, D. K., Knösche, T. R. & Turner, R. White matter integrity, fiber count, and other
763 fallacies: The do's and don'ts of diffusion MRI. *Neuroimage* **73,** 239–254 (2013).

764 27. Brown, M. W., Warburton, E. C. & Aggleton, J. P. Recognition memory: Material, processes,
765 and substrates. *Hippocampus* **20,** 1228–1244 (2010).

766 28. Diana, R. A., Yonelinas, A. P. & Ranganath, C. Imaging recollection and familiarity in the
767 medial temporal lobe: a three-component model. *Trends Cogn. Sci.* **11,** 379–386 (2007).

768 29. Gross, M. M. Hemispheric specialization for processing of visually presented verbal and
769 spatial stimuli. *Percept. Psychophys.* **12,** 357–363 (1972).

770 30. Nagel, B. J., Herting, M. M., Maxwell, E. C., Bruno, R. & Fair, D. Hemispheric lateralization of
771 verbal and spatial working memory during adolescence. *Brain Cogn.* **82,** 58–68 (2013).

772 31. Papanicolaou, A. C. *et al.* The Hippocampus and Memory of Verbal and Pictorial Material.
773 *Learn. Mem.* **9,** 99–104 (2002).

774 32. Ranganath, C. & Ritchey, M. Two cortical systems for memory-guided behaviour. *Nat. Rev.*
775 *Neurosci.* **13,** 713 (2012).

776 33. Doty, R. W., Ringo, J. L. & Lewine, J. D. Forebrain commissures and visual memory: a new
777 approach. *Behav. Brain Res.* **29,** 267–80 (1988).

778 34. Lewine, J. D., Doty, R. W., Astur, R. S. & Provencal, S. L. Role of the forebrain commissures in
779 bihemispheric mnemonic integration in macaques. *J Neurosci* **14,** 2515–2530 (1994).

780 35. Botez-Marquard, T; Botez, M. Memory Deficits After Damage to the Anterior Commissure
781 and. *Arch. Neurol.* **49,** 321–324 (1987).

782 36. Gur, R. C. *et al.* A cognitive neuroscience-based computerized battery for efficient
783 measurement of individual differences: Standardization and initial construct validation. *J.*
784 *Neurosci. Methods* **187,** 254–262 (2010).

785 37. Ritchie, S. J. *et al.* Sex Differences in the Adult Human Brain: Evidence from 5216 UK Biobank
786 Participants. *Cereb. Cortex* **28,** 2959–2975 (2018).

787 38. Ota, M. *et al.* Age-related degeneration of corpus callosum measured with diffusion tensor
788 imaging. *Neuroimage* **31,** 1445–1452 (2006).

789 39. Sullivan, E. V., Rohlfing, T. & Pfefferbaum, A. Quantitative fiber tracking of lateral and
790 interhemispheric white matter systems in normal aging: Relations to timed performance.
791 *Neurobiol. Aging* **31,** 464–481 (2010).

792 40. Trenerry, M. R. *et al.* MRI hippocampal volumes and memory function before and after
793 temporal lobectomy. *Neurology* **43,** 1800 LP-1800 (1993).

794 41. Dupont, S. Imaging memory and predicting postoperative memory decline in temporal lobe
795 epilepsy: Insights from functional imaging. *Rev. Neurol. (Paris).* **4620,** 201 YP-325 (2015).

796 42. Rosenzweig, I., Beniczky, S., Brunnhuber, F., Alarcon, G. & Valentin, A. The Dorsal
797 Hippocampal Commissure: When Functionality Matters. *J. Neuropsychiatry Clin. Neurosci.* **23,**
798 E45–E48 (2011).

799 43. Miró, J. *et al.* Interhemispheric microstructural connectivity in bitemporal lobe epilepsy with
800 hippocampal sclerosis. *Cortex* **67,** 106–121 (2015).

801 44. Smith, S. M. *et al.* Tract-based spatial statistics: Voxelwise analysis of multi-subject diffusion
802 data. *Neuroimage* **31,** 1487–1505 (2006).

803 45. Bozzali, M. *et al.* Anatomical connectivity mapping: A new tool to assess brain disconnection
804 in Alzheimer's disease. *Neuroimage* **54,** 2045–2051 (2011).

805 46. Lyksborg, M. *et al.* Secondary progressive and relapsing remitting multiple sclerosis leads to
806 motor-related decreased anatomical connectivity. *PLoS One* **9,** (2014).

807 47. Vos, S. B., Jones, D. K., Viergever, M. A. & Leemans, A. Partial volume effect as a hidden

808 covariate in DTI analyses. *Neuroimage* **55,** 1566–1576 (2011).

809 48. Dyrby, T. B. *et al.* An ex vivo imaging pipeline for producing high-quality and high-resolution
810 diffusion-weighted imaging datasets. *Hum. Brain Mapp.* **32,** 544–563 (2011).

811 49. Dyrby, T. B. *et al.* Interpolation of diffusion weighted imaging datasets. *Neuroimage* **103,**
812 202–213 (2014).

813 50. Dyrby, T. B., S⃠gaard, L. V, Hall, M. G., Ptito, M. & Alexander, D. C. Contrast and stability of
814 the axon diameter index from microstructure imaging with diffusion MRI. *Magn. Reson. Med.*
815 **70,** 711–721 (2013).

816 51. Cook, P. A. *et al.* Camino: Open-source diffusion-MRI reconstruction and processing. *Camino*
817 *Open-Source Diffus. Reconstr. Process.* (2006).

818 52. Woods, R. P. *et al.* A web-based brain atlas of the vervet monkey, Chlorocebus aethiops.
819 *Neuroimage* **54,** 1872–1880 (2011).

820 53. Glasser, M. F. *et al.* The minimal preprocessing pipelines for the Human Connectome Project.
821 *Neuroimage* **80,** 105–124 (2013).

822 54. Sotiropoulos, S. N. *et al.* Effects of image reconstruction on fiber orientation mapping from
823 multichannel diffusion MRI: Reducing the noise floor using SENSE. *Magn. Reson. Med.* **70,**
824 1682–1689 (2013).

825 55. Van Essen, D. C. *et al.* The WU-Minn Human Connectome Project: An overview. *Neuroimage*
826 **80,** 62–79 (2013).

827 56. Mugler, J. P. & Brookeman, J. R. Three-dimensional magnetization-prepared rapid gradient-
828 echo imaging (3D MP RAGE). *Magn. Reson. Med.* **15,** 152–157 (1990).

829 57. Jenkinson, M. & Smith, S. A global optimisation method for robust affine registration of brain
830 images. *Med. Image Anal.* **5,** 143–156 (2001).

58. Jenkinson, M., Bannister, P., Brady, M. & Smith, S. Improved Optimization for the Robust and Accurate Linear Registration and Motion Correction of Brain Images. *Neuroimage* **17,** 825–841 (2002).

59. Weintraub, S. *et al.* Cognition assessment using the NIH Toolbox. *Neurology* **80,** S54 LP-S64 (2013).

60. Klingler, J. & Gloor, P. The connections of the amygdala and of the anterior temporal cortex in the human brain. *J. Comp. Neurol.* **115,** 333–369 (1960).

61. Turner, B. H., Mishkin, M. & Knapp, M. E. Distribution of the anterior commissure to the amygdaloid complex in the monkey. *Brain Res.* **162,** 331–337 (1979).

62. Smith, S. M. *et al.* Advances in functional and structural MR image analysis and implementation as FSL. *Neuroimage* **23,** 208–219 (2004).

63. Dyrby, T. B., Innocenti, G. M., Bech, M. & Lundell, H. Validation strategies for the interpretation of microstructure imaging using diffusion MRI. *Neuroimage* (2018). doi:https://doi.org/10.1016/j.neuroimage.2018.06.049

64. Fedorov, A., Li, X., Pohl, K.M., Bouix, S., Styner, M., Addicott, M., Wyatt, C., Daunais, J.B., Wells, W.M., & Kikinis, R. Atlas-Guided Segmentation of Vervet Monkey Brain MRI. *Open Neuroimag. J.* **5,** 186–197 (2011).

65. Johnson, H., Harris, G. & Williams, K. BRAINSFit: Mutual Information Rigid Registrations of Whole-Brain 3D Images, Using the Insight Toolkit. *Insight J.* 1–10 (2007).

66. Pohl, K. M. *et al.* A hierarchical algorithm for MR brain image parcellation. *IEEE Trans. Med. Imaging* **26,** 1201–1212 (2007).

67. Leemans, A., Jeurissen, B., Sijbers, J. & Jones, D. ExploreDTI: a graphical toolbox for processing, analyzing, and visualizing diffusion MR data. *Proc. 17th Sci. Meet. Int. Soc. Magn.*

854 *Reson. Med.* **17,** 3537 (2009).

855 68. Tournier, J.-D. *et al.* Resolving crossing fibres using constrained spherical deconvolution:
856 Validation using diffusion-weighted imaging phantom data. *Neuroimage* **42,** 617–625 (2008).

857 69. Jeurissen, B., Leemans, A., Jones, D. K., Tournier, J.-D. & Sijbers, J. Probabilistic fiber tracking
858 using the residual bootstrap with constrained spherical deconvolution. *Hum. Brain Mapp.* **32,**
859 461–479 (2011).

860 70. Patenaude, B., Smith, S. M., Kennedy, D. N. & Jenkinson, M. A Bayesian model of shape and
861 appearance for subcortical brain segmentation. *Neuroimage* **56,** 907–922 (2011).

862 71. Jeurissen, B., Tournier, J.-D., Dhollander, T., Connelly, A. & Sijbers, J. Multi-tissue constrained
863 spherical deconvolution for improved analysis of multi-shell diffusion MRI data. *Neuroimage*
864 **103,** 411–426 (2014).

865 72. Cohen, J. *Statistical Power Analysis for the Behavioral Sciences*. *Routledge Academic*
866 (Lawrence Erlbaum Associates, Publishers, 1988). doi:10.2307/2529115

867 73. Voevodskaya, O. *et al.* The effects of intracranial volume adjustment approaches on multiple
868 regional MRI volumes in healthy aging and Alzheimer's disease . *Frontiers in Aging*
869 *Neuroscience* **6,** 264 (2014).

870 74. Kanaan, R. A. *et al.* Gender influence on white matter microstructure: A tract-based spatial
871 statistics analysis. *PLoS One* **9,** 1–6 (2014).

872 75. León, I., Tascón, L. & Cimadevilla, J. M. Age and gender-related differences in a spatial
873 memory task in humans. *Behav. Brain Res.* **306,** 8–12 (2016).

874 76. Luders, E., Gaser, C., Narr, K. L. & Toga, A. W. Why Sex Matters: Brain Size Independent
875 Differences in Gray Matter Distributions between Men and Women. *J. Neurosci.* **29,** 14265–
876 14270 (2009).

877